

A system to impose prescribed homogenous strains on cultured cells

CHRISTOPHER M. WATERS,^{1,2} MATTHEW R. GLUCKSBERG,¹
EUGENE P. LAUTENSCHLAGER,³ CHYH-WOEI LEE,¹ REED M. VAN MATRE,¹
RICHARD J. WARP,¹ USHMA SAVLA,¹ KEVIN E. HEALY,^{1,3} BRIAN MORAN,⁴
DAVID G. CASTNER,⁵ AND JANE P. BEARINGER^{1,3}

¹Biomedical Engineering and ⁴Civil Engineering Departments, McCormick School of Engineering and Applied Science, Northwestern University, Evanston, Illinois 60208; ²Department of Physiology, The University of Tennessee Health Science Center, Memphis, Tennessee 38163; ³Division of Biological Materials, Dental School, Northwestern University, Chicago, Illinois 60611; and ⁵NESAC/BIO, Department of Chemical Engineering and Center for Bioengineering, University of Washington, Seattle, Washington 98195

Received 27 December 2000; accepted in final form 4 June 2001

Waters, Christopher M., Matthew R. Glucksberg, Eugene P. Lautenschlager, Chyh-Woei Lee, Reed M. Van Matre, Richard J. Warp, Ushma Savla, Kevin E. Healy, Brian Moran, David G. Castner, and Jane P. Bearinger. A system to impose prescribed homogenous strains on cultured cells. *J Appl Physiol* 91: 1600–1610, 2001.—There is presently significant interest in cellular responses to physical forces, and numerous devices have been developed to apply stretch to cultured cells. Many of the early devices were limited by the heterogeneity of deformation of cells in different locations and by the high degree of anisotropy at a particular location. We have therefore developed a system to impose cyclic, large-strain, homogeneous stretch on a multi-well surface-treated silicone elastomer substrate plated with pulmonary epithelial cells. The pneumatically driven mechanism consists of four plates each with a clamp to fix one edge of the cruciform elastomer substrate. Four linear bearings set at predetermined angles between the plates ensure a constant ratio of principal strains throughout the stretch cycle. We present the design of the device and membrane shape, the surface modifications of the membrane to promote cell adhesion, predicted and experimental measurements of the strain field, and new data using cultured airway epithelial cells. We present for the first time the relationship between the magnitude of cyclic mechanical strain and the extent of wound closure and cell spreading.

airway epithelial cells; biaxial strain; surface chemistry; cellular biomechanics

IN RECENT YEARS THERE HAS been a proliferation of devices intended to provide a mechanical environment for cultured cells similar to that which occurs in vivo (3). Early efforts focused on the behavior of endothelial cells under the influence of continuous fluid shear as an approximation of the stresses imposed by the flow of blood through vessels (reviewed in Ref. 8), and this

avenue of study has continued with increasingly sophisticated devices for imposing known and time-varying shear stress. Other investigators have begun to examine the effects of stretch on cultured cells, including vascular endothelial cells (11, 28, 36), smooth muscle cells (7, 29), fibroblasts (5, 30), osteoblasts (26), fetal lung cells (18, 19), and other cells (1, 2, 33, 34).

As with all in vitro systems, and indeed all physiological models, each technique has its limitations, and these have been reviewed extensively by Brown (3). The most widely used system for applying cyclic stretch is the commercially available Flexercell strain unit (Flexcell International, McKeesport, PA), in which a vacuum applied under the membrane deforms the monolayer of cells grown on top of the membrane. Our laboratory utilized the Flexercell apparatus to demonstrate strain-induced inhibition of prostanoid synthesis (24) and wound closure (25) in airway epithelium. The many attractive features of the Flexercell unit (ease of use, reliability, multiple wells, availability) promoted its use, but its utility was initially limited by the high degree of anisotropy and heterogeneity of the deformations. Anisotropy occurs when the magnitude of strain at a particular location varies in different axial directions. Heterogeneity occurs when the strain tensor varies with position. Similar units have been designed to operate with a positive pressure (12, 36), which generally results in a more homogeneous deformation of the cell monolayer (3) but is still far from isotropic or homogeneous over the entire surface. Other investigators have constructed devices that avoid nonuniform deformation by restricting the deformations to uniaxial stretch (5, 7, 20, 30). Still others have approached the problem with devices to provide a better approximation of a uniform biaxial strain field;

Address for reprint requests and other correspondence: C. M. Waters, Dept. of Physiology, The Univ. of Tennessee Health Science Center, 894 Union Ave., Nash 426, Memphis, TN 38163 (E-mail: cwaters@physiol.utm.edu).

The costs of publication of this article were defrayed in part by the payment of page charges. The article must therefore be hereby marked "advertisement" in accordance with 18 U.S.C. Section 1734 solely to indicate this fact.

however, in many cases these either were not designed for cyclic stretch or were not suitable for use in an incubator (21). Vandenburg (32) developed a narrow prong-displacement system although no strain distribution was reported. Similar systems using a glass dome (1, 4), platen (6, 26, 27), or a ring (15, 17, 31) instead of a narrow prong have been shown to impose more highly uniform and isotropic deformations. The system described by Schaffer et al. (26) and Cheng et al. (6), in particular, achieved an impressive strain up to 33% that was nearly isotropic and homogeneous. The manufacturer of the Flexercell device has modified the well design for the plates (BioFlex-II) so that the diameter is larger (36 mm) and the thickness of the membrane is reduced (0.5 mm), leading to much improved radial strain homogeneity. In addition, the company now markets a fixed loading station that simulates the platen-loading systems by applying a vacuum only in the outer annulus of the well, causing the membrane to distend uniformly over the loading station. One disadvantage of these systems is that the sliding of the membrane over the platen or loading station causes friction that might lead to increased heating of the cultured cells. Another disadvantage is that there is little flexibility in terms of controlling anisotropy, if that is a feature that is desired.

We report a practical system designed and constructed for stretching cultured cells that overcomes some of the limitations of previous efforts. Our device has two mechanical components. One, which we call the "rack," is a pneumatically driven mechanism that imposes a known set of displacements at a prescribed rate. The second mechanical component is the elastomer substrate or "membrane," which is fixed in the rack and stretched to impose a prescribed set of strains. We present our characterization of the membrane mechanical characteristics, surface modification for cell culture, finite element analysis of the strain field, and experimental measurements of the strain field. In addition, we present initial data using cultured airway epithelial cells, which demonstrate that uniform biaxial cyclic stretch inhibits prostanoic synthesis and wound closure. We report for the first time that the inhibition of wound closure was dependent on the magnitude of strain.

METHODS

Mechanical design and design considerations. The device was designed to satisfy several performance criteria. First and foremost, homogeneity of deformations over the surface of the wells should be maintained as tightly as possible. The other important consideration was the ability to maintain and control the degree of isotropy within the wells. Additional design considerations were the ability to vary the degree of strain anisotropy; the ability to control the frequency, duty cycle, strain rate, and magnitude of the oscillations independently; and the ability to ultimately use this device with a permeable substrate. The latter design consideration was imposed because we wish to eventually culture airway epithelial cells at an air-liquid interface, which is not possible with the Flexercell device or any of the commercially available deflection-type devices.

A computer-generated drawing of the device is shown in Fig. 1 in the relaxed (A) and in the distended (B) states, and a photograph of the device with an elastomer membrane clamped in place is shown (C). The rack is a pneumatically driven mechanism compact enough to fit inside an incubator and consists of four ¼-in.-thick aluminum plates (two 4 × 11 in., one 3 × 22 in., and one 2 × 20 in.) each with a clamp to fix one edge of the cruciform membrane. The clamps were lined with sandpaper to prevent slippage of the membrane. Four linear bearings set at predetermined angles between the plates ensure a constant ratio of principal strains throughout the stretch cycle, and in the drawing shown in Fig. 1 the ratio is set at one. The ratio may be varied simply by replacing the two side plates so that the linear bearings are set at an arbitrary angle between 0 and 45°. The frequency of the oscillatory stretch is set between 1 and 0.01 Hz by computer-controlled electronic valves connecting a 100-psi compressed air source to the pneumatic actuators, and the computer also controls the duty cycle. The rates of extension and relaxation are independently controlled by the computer by use of electronic needle valves. In most experiments described below, cyclic stretch was applied with a frequency of 30 cycles/min with strain applied for 1 s during each cycle. The strain rate was set at ~50%/s so that maximal distention (10%) was obtained within 0.2 s. The magnitude of the strains is set by a mechanical stop.

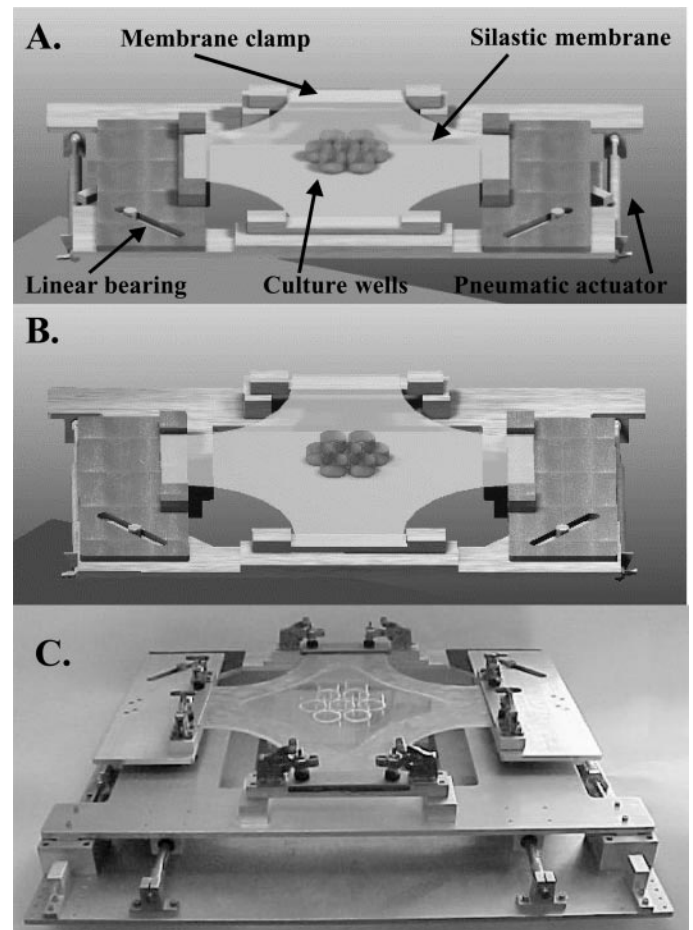


Fig. 1. Computer-generated drawing of the mechanical design of the device, showing the mechanism for converting the 1-dimensional motion of the pneumatic actuators into biaxial stretch of the relaxed (A) and distended (B) silicone rubber membrane. C: photograph of the device with the elastomer membrane in the relaxed state.

Membrane manufacture and preparation. The elastomer membrane was manufactured by using Dow Corning (Midland, MI) Silastic T-2 mixed at a 10:1 base-catalyst ratio. The base-catalyst mixture was poured directly into a mold fashioned from cast acrylic (Plexiglas) and smoothed to a uniform thickness of ~ 2.5 mm. Within the first hour of curing, any large bubbles were punctured to prevent defects in the cured membrane. Well walls were formed separately by partially filling 2.5-cm ID centrifuge tubes with the uncured Silastic mixture, inverting the tubes on a rack, and allowing the excess Silastic to coat the inside surfaces. When fully cured, the 0.1-mm thick elastomer linings were peeled from the centrifuge tubes and cut into 12-mm ring segments to form the well walls. The well walls were then placed on the partially cured membrane and left for 24 h to complete the curing process.

The shape, thickness of the membrane, and placement of the wells on the membrane were determined by an iterative process using prototypes and finite element models. We determined the uniaxial material properties of the Silastic by testing a $5 \times 10 \times 0.25$ mm rectangular strip in an Instron testing machine (floor model 1114, Canton, MA). From uniaxial tests, the material is well characterized as a Blatz-Ogden material with a strain energy density function per unit initial volume, W , under conditions of plane stress, given by

$$W = 2\mu(\lambda_1^{-\alpha} + \lambda_2^{-\alpha} + \lambda_1^\alpha \lambda_2^\alpha - 3)/\alpha^2 \quad (1)$$

where λ_1 and λ_2 are the stretch ratios and α and μ are material constants determined to be 0.3 and 5.5×10^6 dyn/cm², respectively. We used ABAQUS (Hibbitt, Karlsson, and Sorensen, Pawtucket, RI), a commercially available finite element package on a Hewlett-Packard 9000 Series 720 Unix workstation, to model the material and predict the local deformations caused by prescribed displacements of the membrane at the clamps. Each proposed membrane geometry was first evaluated by finite element analysis, and membrane geometries were adjusted by varying element distribution, sizes, and thicknesses. The analysis included the placement of the wells on the top surface and consideration of their contribution to the material response. The membrane geometry was optimized for intrawell and interwell homogeneity and isotropy over a wide range of equibiaxial stretch. To assure numerical stability and accuracy, the size of the finite element mesh was increased until variations in maximum principal strains were $<1\%$. To validate the predictions of our finite element analysis, we printed a mesh on an acetate transparency by using a 300 dpi laser printer (HP Laserjet II) but stopped the page feed before the page passed over the heating element. The transparency with the unfused toner attached was then trimmed and placed toner side up in the mold, and the Silastic was poured and cured as described above. Thus the finite element mesh was transferred precisely and indelibly to the membrane itself. Displacements were recorded by a charge-coupled device camera (Hamamatsu, Hamamatsu City, Japan) and a personal computer-based image processing system (Metamorph, Universal Imaging, West Chester, PA) and were compared with the finite element predictions. Positions of features (lines of toner) on the membranes were extracted from captured images by an algorithm that fit the image intensity across a line to an even-ordered polynomial function. The pixel closest to the midpoint of the polynomial was considered to be the centerline. The positions in the deformed (stretched) configuration were used to calculate displacements u_i with respect to the original configuration described by the coordinates a_i . The

quantities were then used to approximate the local Green's strains E_{ij} and stretch ratios λ_k using the relation

$$E_{ij} = \frac{1}{2}[\partial u_i/\partial a_j + \partial u_j/\partial a_i + (\partial u_i/\partial a_k)(\partial u_j/\partial a_k)] \quad (2)$$

where u_i/a_j may be approximated by a linear interpolation function between nodes. Stretch ratios λ_1 and λ_2 were computed from the relation $\lambda_k = (2E'_{ij} + 1)^{1/2}$, where E'_{ij} are the principal components of E_{ij} . For comparisons to the finite element model presented in the RESULTS section, we limited the nodes examined to those within the wells.

Membrane surface modification and characterization. To facilitate protein adsorption and cell adhesion, the membranes were exposed to an oxygen plasma by use of methods adapted from Ferguson et al. (9). The oxygen plasma was used to form a thin layer of oxidized silicon (SiO_x) on the disordered silicone membranes that was amenable to further modification with organosilanes. Oxygen plasma conditions were varied and optimized to avoid altering the mechanical properties of the membranes. Membranes were exposed to an oxygen plasma (March Plasmod, Concord, CA) at 0.4 Torr oxygen pressure and 45 W power for either 30, 60, or 90 s. An aminosilane [*N,N*-2-aminoethyl-3-aminopropyl trimethoxysilane (EDS), Hüls America, Piscataway, NJ] was coupled to the oxidized membrane in the following manner. A solution of 1% EDS and 94% anhydrous methanol (1 mM acetic acid in methanol) was prepared in a glove box under nitrogen atmosphere. The beaker was transferred into a laminar flow fume hood (Class 100), and 5% ultrapure water was added. The solution was mixed, and the membrane wells were filled with the solution for 5 min and then rinsed three times in methanol for 1 min each rinse. Membranes were sterilized by use of ethanol.

To verify the surface modification, membrane chemistry and species present were analyzed using X-ray photoelectron spectroscopy (XPS), also known as electron spectroscopy for chemical analysis. This is an extremely sensitive technique that probes the chemical composition of the outer 1–15 nm of a surface (e.g., the membrane). XPS is based on the photoemission of core-level electrons in an atom, and the principles of the technique are reviewed in detail by Ratner and McElroy (22) and Grainger and Healy (13). XPS analyses were conducted on a Surface Science Instrument (SSI) X-probe spectrometer with a monochromatic Al K_{α1,2} X-ray source (1486.6 eV) to stimulate photoemission. Emitted electron energies were measured with a hemispherical energy analyzer at pass energies ranging from 25 to 150 eV. Binding energy was referenced by setting the CH_x peak maximum in the C1s spectrum to 285.0 eV. Survey and high-resolution spectra were collected at a takeoff angle of 55° (the take-off angle, ϕ , is defined as the angle between the surface normal and the axis of the analyzer lens system). Survey spectra were collected over a binding energy range of 0–1,000 eV, high-resolution C1s spectra were collected over a 275- to 295-eV range, and Si2p spectra were collected over a 96- to 108-eV window. Analyzer resolution was on the order of 1.5 eV for survey scans and 0.25 eV for high-resolution scans. SSI data analysis software was used to calculate elemental compositions from peak areas and to peak-fit the high-resolution spectra.

1HAEo⁻ and 16HBE14o⁻ cell culture. Airway epithelial cells transformed with the SV₄₀ virus (1HAEo⁻ and 16HBE14o⁻) were provided by Dr. D. Gruenert (University of California-San Francisco) and have been characterized by his laboratory (14). Cells were grown in modified Eagle's medium containing 10% FBS, 2 mM L-glutamine, 100 μg/ml streptomycin, and 100 U/ml penicillin G. To further promote cell adhesion, the membranes were coated with type I rat tail collagen (50

$\mu\text{g/ml}$ in 2.5% acetic acid for 15 min). Cells were seeded onto the membranes at $2\text{--}3 \times 10^5$ cells/well and used on *day 4* of culture.

Prostaglandin E_2 measurement. PGE_2 synthesis by cyclically stretched 1HAEo⁻ cells was assessed by collecting media samples 5, 10, and 20 min after the initiation of cyclic stretch. PGE_2 was analyzed by a sensitive and highly specific competitive enzyme immunoassay from Cayman Chemical (Ann Arbor, MI). The quantity of PGE_2 measured was normalized to the average cell number.

Wounding protocol and measurement of cell area and centroid-centroid distance. Confluent monolayers of 1HAEo⁻ or 16HBE14o⁻ cells were wounded by scraping the monolayers with a metal spatula across the diameter of the well. Duplicate paired membranes were either subjected to cyclic strain using the biaxial stretcher or maintained static as a control. The frequency of strain was 30 cycles/min (1 s stretch/1 s relaxation per cycle), and elongation and compression were varied. In the compression studies, cells were cultured on a prestretched membrane before wounding, and then cyclic "relaxation" of the membrane led to compression of the cells. After wounding, the cells were rinsed once with PBS to remove cellular debris. Complete growth medium (2 ml) was added to the wells, and this medium was not removed during

the course of the experiment. Images were obtained at the initial time of wounding and at various times up to 24 h postwounding. Images of the wounds were obtained across the entire well. Cell area and centroid-centroid distance between cells were measured by tracing cells at the wound edge as previously described (35).

RESULTS

Device performance. The device performs well and meets all our design criteria. The simplicity of the pneumatic-driven rack mechanism and the choice of noncorroding materials ensure reliability in the warm and humid environment of an incubator. The aluminum base and stainless steel bearings have run routinely for periods of 24–48 h without problems. The design is modular, so failure due to wear can easily be repaired by replacing individual, easily fabricated elements. One of our design criteria was to allow for stretch that was of arbitrary but prescribed anisotropy. We achieved that by swapping out the side plates so that the bearings were aligned at 60° and near 90° angles rather than the 45° angles shown in Fig. 1. This

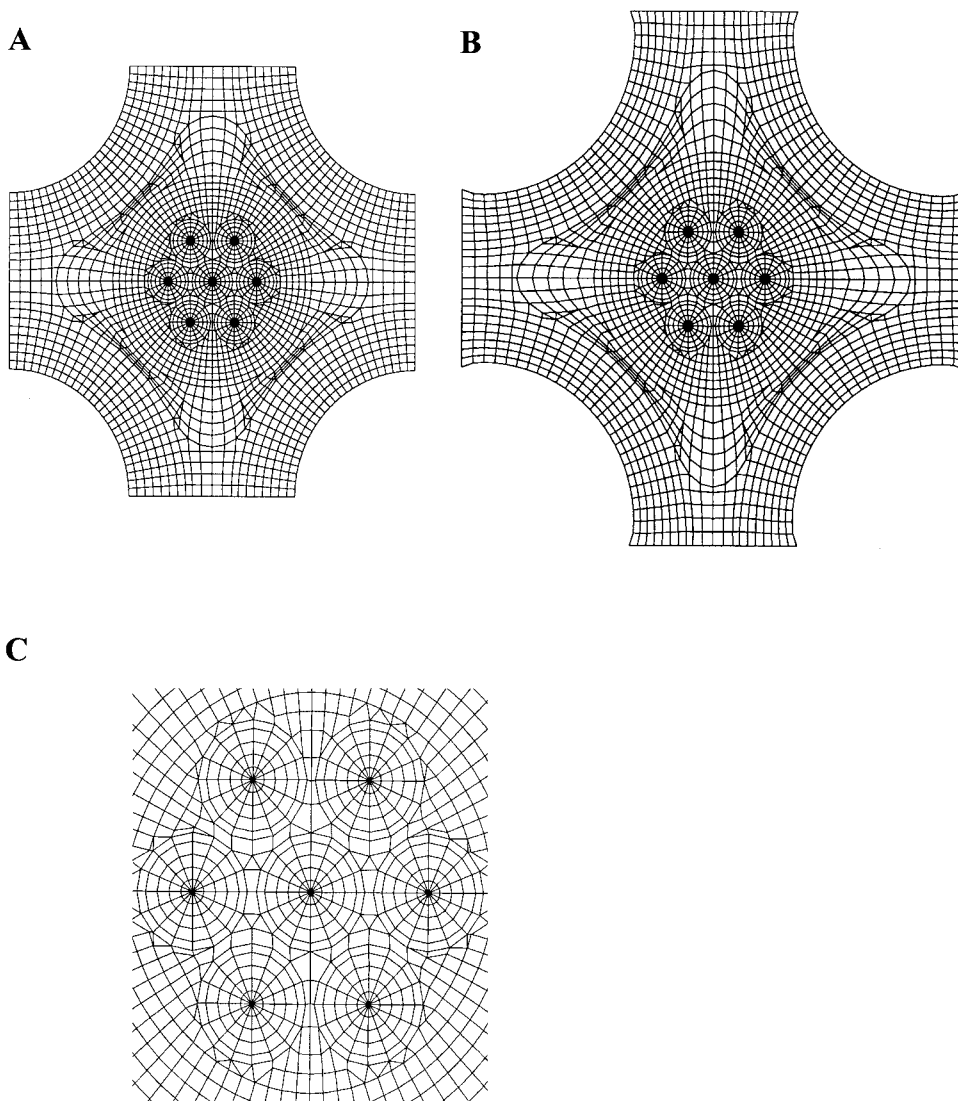


Fig. 2. Finite element mesh used to design the silicone rubber membrane that acts as an extensible substrate for cultured cells in its unstretched (*A*) and stretched configuration (15% well strain; *B*). Boundary conditions are a mixture of stress-free (along the curved edges) and prescribed displacement (along the clamped, straight edges). *C*: finite element grid when anisotropic strain was applied. In this case, a 15% stretch was applied in the vertical direction while no strain was applied in the horizontal direction.

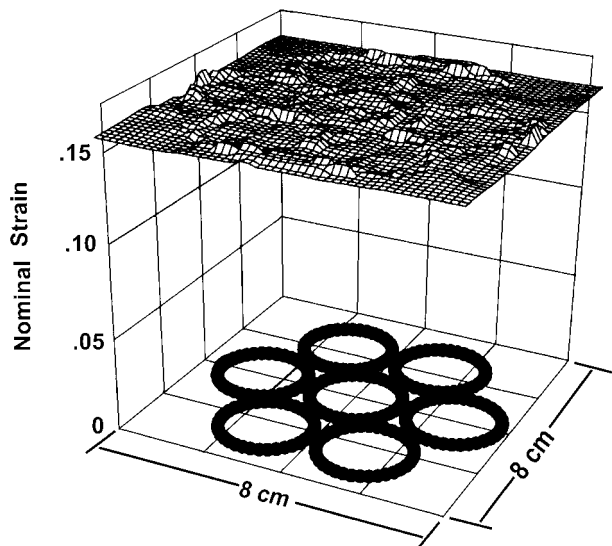


Fig. 3. The finite element model predicts a uniform and isotropic distribution of strain over the central portion of the membrane. Effects of the well walls on the strain distribution can be seen as the raised "rims" on this graph.

feature allows for strain to remain homogeneous over the surface of the wells but maintains a fixed level of isotropy. In the case in which the angle is set closer to 90° , true uniaxial strain is achievable, in contrast to some other devices that apply uniaxial stress and cause compression in the in-plane transverse direction.

Membrane mechanics. A membrane of uniform thickness mounted in the rack and symmetrically stretched will only undergo isotropic and homogeneous large strain in a relatively small region near the center of the membrane. We therefore used finite element analysis to design a membrane with a thin central region surrounded by a thicker peripheral region and shaped with generous curves so as to optimize the three factors of interest within the wells: strain magnitude, strain isotropy, and strain homogeneity. The finite element grid and membrane geometry that resulted from this ad hoc and iterative process is shown in Fig. 2 in the unstretched state (Fig. 2A) and with 15% strain (Fig.

2B). As an example of anisotropic strain, Fig. 2C demonstrates the changes in the finite element grid for 15% strain in the vertical direction with no strain in the horizontal direction. The outer portion of the membrane was fixed at a thickness of 4.4 mm, whereas the inner portion of the membrane (including the wells) was fixed at 2.2 mm. Because the walls of the wells and the Silastic used to attach them to the membrane contribute to the thickness, we made a cross-sectional cut of a membrane and measured the thickness. The thicknesses at each location were input into the finite element analysis. Figure 3 shows the predicted strain field in the wells for isotropic strain.

To validate the finite element method we also present measurements taken directly from the membrane itself for comparison to the model-predicted results in Fig. 3. Figure 4 shows photographs of a portion of the finite element grid indelibly marked on the Silastic surface on the unstretched membrane and on the membrane stretched 15% in three different wells. Similar images were used to measure the strain field in the wells shown in Fig. 4 and show an acceptably uniform strain profile both within and between wells (Fig. 5). Also shown in Fig. 5 are the predicted strain profiles. We note that the predicted deformations are consistently 1–2% higher than those measured experimentally; this may be attributed to some degree of slip at the clamped edge. We also noted some minor plastic deformation in high-strain regions of the membrane. We chose the strain energy density function, *Eq. 1*, on the basis of results of uniaxial testing of the Silastic membrane. More extensive testing of the material under multiaxial conditions might lead to some adjustment of the material parameters with a slight effect on the predicted strain field, but a perfect fit between theory and experiment was not the goal of this analysis. The model returns reasonable values for strain and serves as a workable method to help guide the design of the membrane. The strains were determined by direct measurement.

Surface characterization. Changes in the surface chemistry due to the modification of the membranes

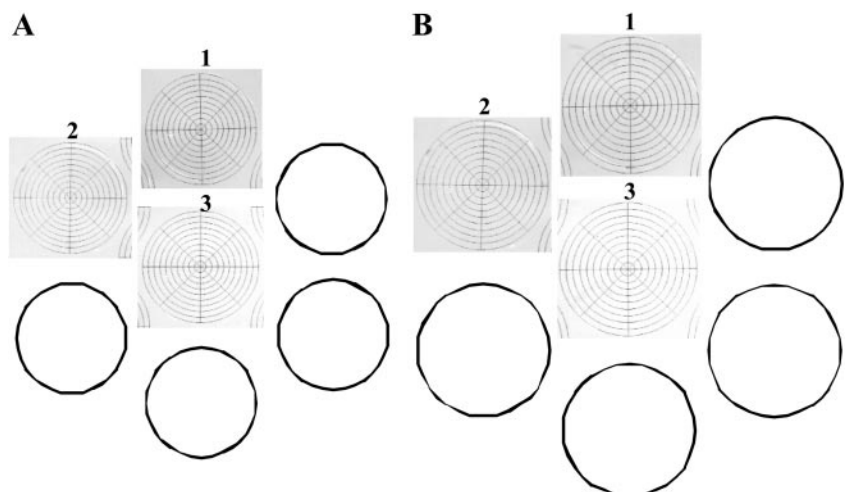


Fig. 4. Portions of the finite element mesh were printed on the membrane under the wells and photographed to assess the uniformity and isotropy of the strain field. Wells remained round and the distance between concentric circles remained equal when the membrane was deformed from its initial configuration (A) to its stretched configuration (B). Three wells are labeled for the strain measurements shown in Fig. 5.

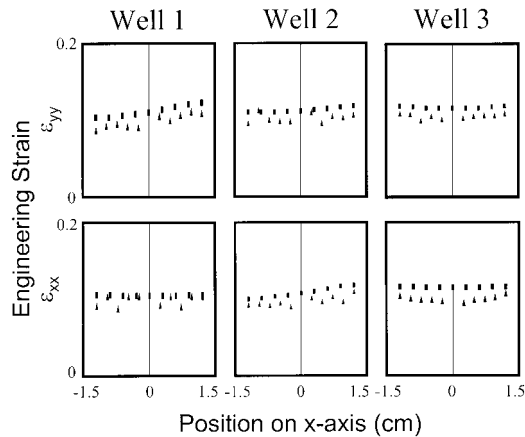


Fig. 5. Experimental measurements and model predictions for wells 1, 2, and 3 as labeled in Fig. 4 but with 10% strain applied. Predicted (■) and measured (▲) strains in wells 1, 2, and 3 along the x-axis of each well. ϵ_{xx} and ϵ_{yy} represent the normal strains in the x and y directions, respectively. Theory consistently overestimates the strains by a few percent.

were determined by XPS. The atomic composition of the surface during each stage of the protocol was determined from XPS survey spectra (Table 1). Treatment of the Silastic membrane with the oxygen plasma led to a time-dependent increase in the oxygen content and a decrease in the carbon present at the surface. Figure 6 shows the high-resolution Si2p spectra, which supports the atomic composition analysis and indicates that silicon oxides, possibly SiO_x, were produced after exposure to the oxygen plasma. Clearly, a shift in the Si2p peak line shape occurred during the plasma treatment: the predominant silicon peak at 102.6 eV for the starting material was replaced by the oxide peak (104 eV) during the plasma treatment. The peak area ratios of the silicon to the oxide species in the Si2p spectra changed from 2.7:1 for the initial Silastic to 1:4 after 90 s oxygen plasma treatment, indicating substantial oxidation of the surface to a depth of ~6 nm. The formation of SiO_x species was a prerequisite for coupling the organosilane, EDS, to the surface. Analysis of high-resolution C1s spectra in Fig. 7 confirmed that the starting membrane had no oxidized carbon species (Fig. 7A), and, after 90 s of exposure in the

Table 1. Elemental surface composition of Silastic membranes at each stage of the treatment as determined by XPS

Sample	XPS Atomic Percent			
	Si	O	C	N
Untreated	27.2	28.0	44.8	
30-s Oxygen plasma	28.2	37.6	34.2	
60-s Oxygen plasma	28.9	54.3	16.8	
90-s Oxygen plasma	29.3	52.7	18.0	
EDS/90-s Oxygen plasma	26.9	33.6	37.5	2.0
EDS/90-s Oxygen plasma/ethanol	18.9	27.4	45.4	8.4

XPS, X-ray photoelectron spectroscopy; EDS, *N,N*-2-aminoethyl-3-aminopropyl trimethoxysilane.

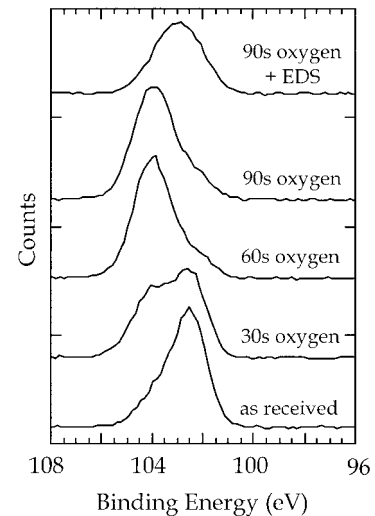


Fig. 6. X-ray photoelectron spectroscopy Si2p spectra for membranes at various stages of the oxygen plasma treatment process. The Si2p line shape shifts from a dominant peak at 102.6 eV for the starting silicone species to 104 eV for the oxidized Si species (e.g., SiO_x). Silicone with an oxidized surface is further modified with an amino-functional organosilane [*N,N*-2-aminoethyl-3-aminopropyl trimethoxysilane (EDS)].

oxygen plasma, oxidized carbon species were also present on the surface (Fig. 7B). Conformation of the immobilization of the EDS was established by the presence of nitrogen in the atomic composition data (Table 1) and the formation of the carbon-nitrogen peak identified in Fig. 7C. Taken together, these data confirm the formation of a thin oxidized surface on the membranes after oxygen plasma treatment and the successful coupling of EDS to the oxidized moieties. Although no quantitative measurements were made, cell adhesion to the membranes was markedly enhanced by the surface treatments. No cells attached to the surfaces before treatment, and excellent cell attachment was observed after treatment.

Response of airway epithelium to stretch. To verify stretching of cell monolayers on the membranes, we constructed a clamping system to fix the membrane in the distended configuration so that cells could be viewed on the microscope. Figure 8 shows Hoffman modulation contrast images of a wounded monolayer of 1HAEo⁻ human airway epithelial cells on an unstretched membrane (Fig. 8A) and after 10% strain (Fig. 8B). The scale bar indicates the separation between the two wound edges. Figure 8, C (unstretched) and D (10% strain), shows higher magnification images of 1HAEo⁻ cells from the same field. Note the expansion of the cluster of cells up and to the right in Fig. 8D.

Our laboratory previously demonstrated that prostanoid release by airway epithelial cells is significantly inhibited by cyclic strain applied using the Flexercell device (24). To verify this response using our biaxial strain device, we cyclically stretched 1HAEo⁻ cells at 10 cycles/min (5-s stretch, 1-s relaxation) with 10% strain. This short relaxation time was previously shown to result in maximal inhibition of prostanoid synthesis. The amount of PGE₂ secreted by the

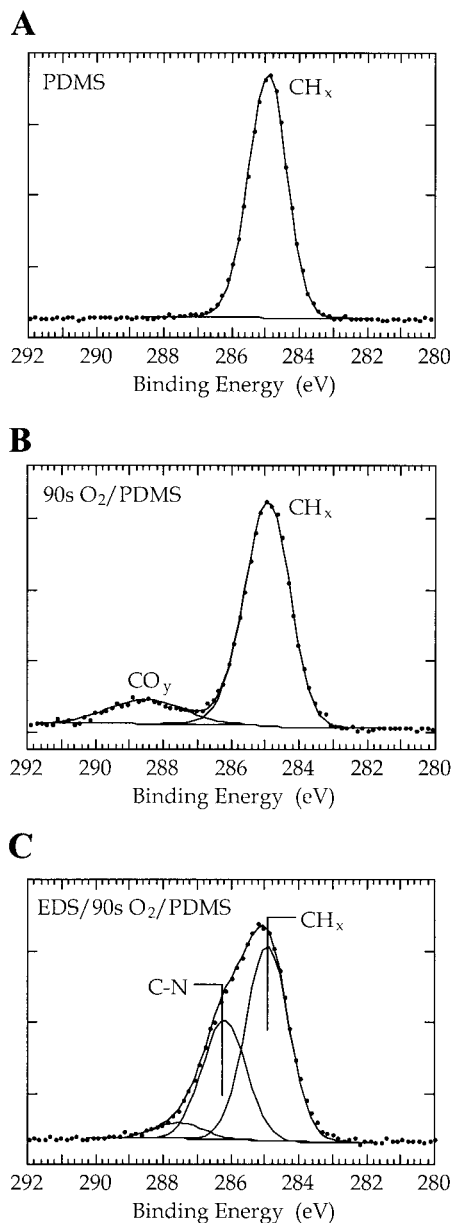


Fig. 7. X-ray photoelectron spectroscopy C1s spectra for membranes. A: spectrum for starting silicone membrane. B: spectrum of 90-s oxygen plasma treatment. C: spectrum after EDS grafting with the peak fit with identical carbon species. PDMS, poly(dimethylsiloxane); CH_x, carbon-hydrogen bonding (x = no. of atoms); C-N, carbon-nitrogen bonding.

stretched cells was inhibited compared with unstretched cells (Fig. 9). Our laboratory also previously demonstrated, using the Flexercell device, that cyclic stretch inhibits wound closure of airway epithelial cells (25). As described in our laboratory's previous study, the distention of the membrane in the Flex-I plates from Flexercell led to radial elongation in the periphery of the wells and radial compression in the center of the wells. Figure 10 shows a comparison of the inhibition of 16HBE14o⁻ wound closure by cyclic mechanical strain using the Flexercell device (Fig. 10A with ~10% mean elongation in the periphery and ~1–2% compres-

sion in the center of the wells) and using our biaxial strain device (Fig. 10B with 10% elongation or with 2% compression). For the compression studies, the cells were cultured on a prestretched membrane before wounding. The membranes were then placed on the stretching device and cyclically relaxed to provide compression to the cells. To further demonstrate the relationship between inhibition of wound closure and the magnitude of mechanical strain, we measured the extent of wound closure after 8 h using our biaxial strain device set for various levels of elongation or compression (Fig. 11). Figure 11 shows that even low levels of compression inhibited wound closure and that maximum inhibition occurred at ~2% compression. To further investigate the inhibitory effect of mechanical strain on wound closure, we measured the cell area at the wound edge as a function of time for each level of strain. Figure 12A shows that cell area increased over time at the wound edge in static cultures but that increasing levels of elongation led to inhibition of cell spreading. At the highest level of elongation studied (9.6%), the cells actually began to decrease in size. By comparison, even the lowest level of compression (0.5%) led to a significant decrease in cell area.

DISCUSSION

Although there has been significant effort to investigate the responses of cultured cells to mechanical strain, many of the existing devices provide strain fields that are both heterogeneous (strain varies from position to position) and anisotropic (strain varies along axial directions at the same location). For example, the radial strain profile of the original Flexercell device varies from maximum tensile strain near the well wall to low levels of compression in the center of the wells, whereas the circumferential strain is near zero at the center and near the walls but is compressive at other radial positions (10). Also, simple uniaxial strain devices may provide uniform strain in one direction, but because of the Poisson effect compression occurs in the transverse direction. In our laboratory's studies examining wound closure of airway epithelium using the Flexercell device (25), we found that compression in the center of the wells inhibited wound closure to a greater extent than elongation in the periphery of the wells (also shown in Fig. 10A). In another study, our laboratory cultured cells in isolated regions of the wells and found that compression resulted in greater inhibition of PGE₂ release than did elongation (24). The compression in the Flexercell device was actually an unwanted characteristic due to the thickness of the membrane that could not be selectively controlled, and cells cultured in the same well were subjected to elongation and compression simultaneously. Therefore, we sought to develop a system in which we could apply both homogeneous and isotropic strain to cultured cells and to apply specific levels of compression. In addition, we wished to have greater control over the surface characteristics of the substrate on which the cells were cultured, and we wished to

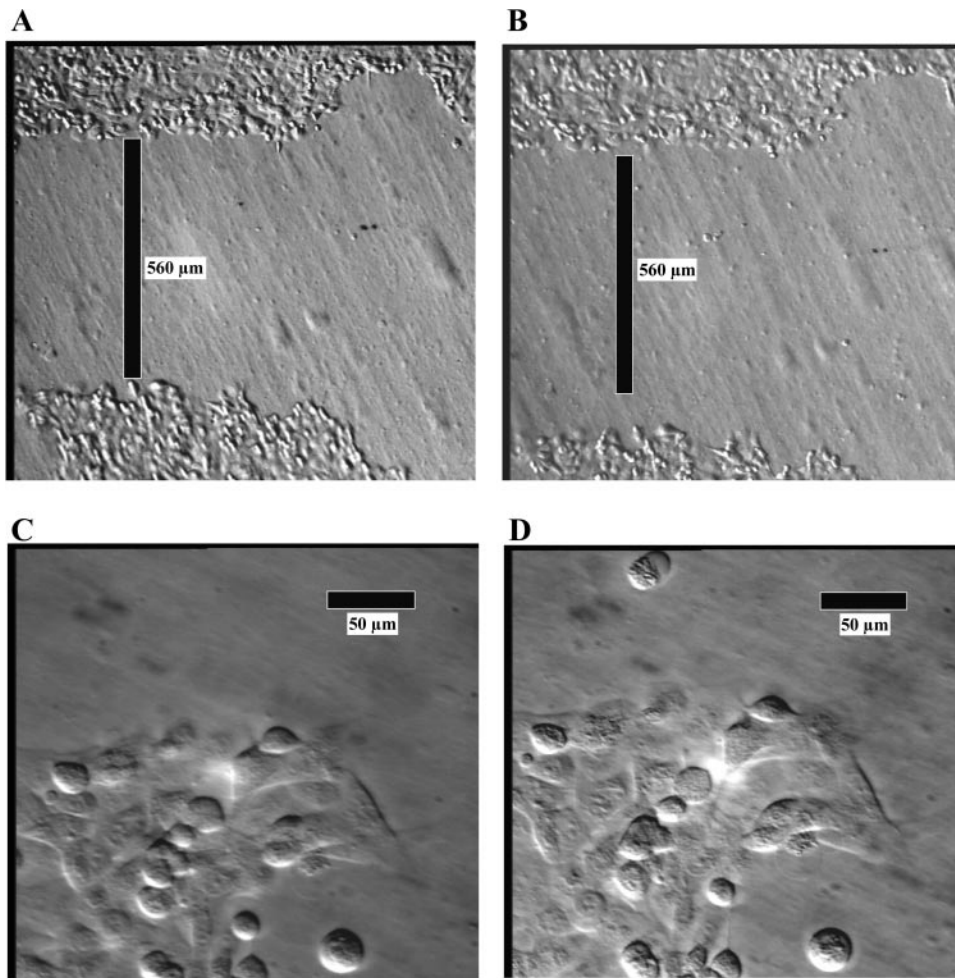


Fig. 8. Hoffman modulation contrast images of human airway epithelial cells (1HAEO⁻) cultured on Silastic membranes. Low-power images of the same wounded monolayer in the unstretched (A) and the stretched condition (B, 10% strain) and higher magnification images of the cells in the unstretched (C) and the stretched condition (D, 10% strain).

have the capability for culturing airway epithelial cells at an air-liquid interface. The present device was developed to meet these criteria. We have not yet achieved the goal of stretching cells cultured at an air-liquid interface, primarily because of material limitations, but our system can be modified for this purpose.

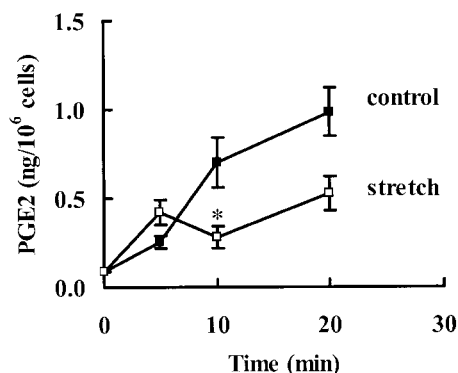


Fig. 9. Cyclic biaxial strain (10% strain, 10 cycles/min, 5-s stretch, 1-s relaxation) inhibited the production of PGE₂ by 1HAEO⁻ cells. Samples were collected at indicated times, and PGE₂ was measured and normalized to cell count. Symbols represent means \pm SE for control (■) and stretched cells (□) from 3 different wells; *significant difference from control ($P < 0.05$).

Our approach is unique among cell-stretching devices in that significant analysis went into the design of the membrane as well as the design of the mechanism used to deform the membrane. We used an iterative finite element-based process to design a membrane that would result in the most uniform strain distribution within the wells. Our model predictions, as shown in Figs. 3 and 5, were useful in designing the shape of the membrane but consistently overestimated the measured strains by 1–2 percentage points. This was likely due to approximating the clamped edges of the membrane by displacement boundary conditions and not accounting for the practical difficulty of imposing such boundary conditions on a soft rubber membrane. By controlling the opening and closing of electronic needle valves, we can control the rate at which strain is applied to the wells as well as the rate of relaxation. This will be useful for studies in which we will mimic the frequency and time-dependent strain experienced by airway epithelial cells during breathing or mechanical ventilation. Because neither side of the well membrane comes in contact with machinery or an applied vacuum or positive pressure where the cells are located, it will eventually be possible to apply strain to cells cultured on a flexible, permeable substrate, allowing for culture of airway epithelial cells at an air-liquid

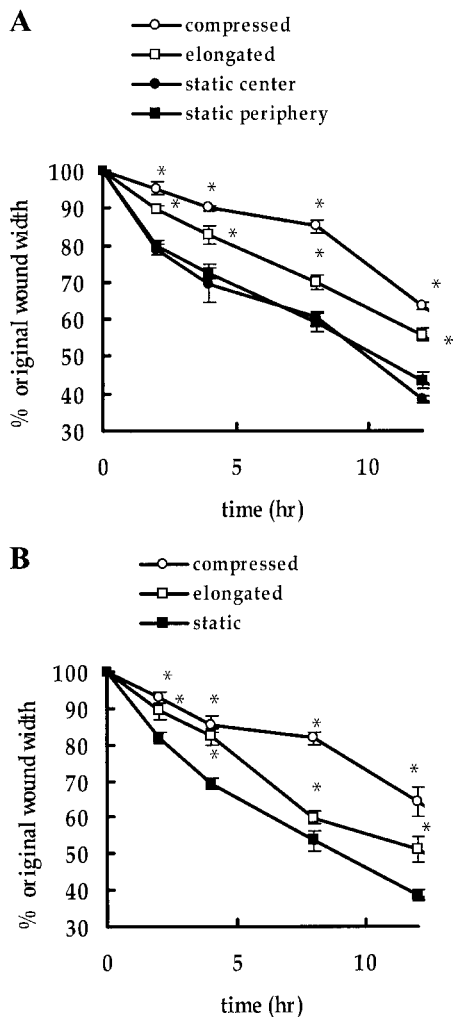


Fig. 10. Comparison of the inhibition of 16HBE140⁻ cell wound closure in the Flexercell device (A) and in our biaxial stretching device (B). In both cases the frequency of strain was 30 cycles/min. Wounds were scraped across the monolayer, and wound widths were measured at the indicated times and normalized to the original wound width. Symbols represent means \pm SE. A: static periphery (\blacksquare), static center (\bullet), elongated (\square), and compressed regions (\circ) from 5 different wells. B: static (\blacksquare), elongated (\square), and compressed (\circ) wells ($n = 5$). *Significant difference from unstretched controls ($P < 0.05$).

interface. Another advantage to our system is that there is no friction due to the sliding of the membrane over a platen or dome surface. The ring loading devices can also avoid the problem of frictional heating by keeping the cell culture areas smaller than the area encompassed by the ring, and these systems can also potentially be used for applying strain to cells on permeable substrates. However, a unique feature of our system is the ability to apply anisotropic strains, as demonstrated in Fig. 2C. Also, the shear stresses that are induced by movement of the fluid over the surface of the cells is estimated to be quite low. With an elongation of 10% and a frequency of 30 cycles/min, we estimate that the maximum shear stress would be ~ 0.025 dyn/cm².

We also developed techniques for controlling the surface chemistry of the silicone elastomer substrate to pro-

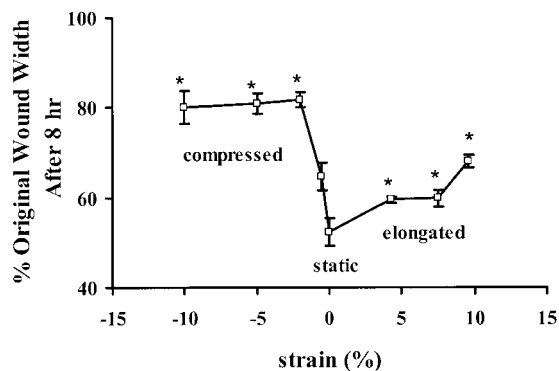


Fig. 11. Inhibition of wound closure in 16HBE140⁻ cells is dependent on the magnitude of cyclic strain. Strain was applied at a frequency of 30 cycles/min. The percentage of the original wound width was measured after 8 h in cultures that had been elongated, compressed, or kept static as indicated ($n = 42$, static; $n = 6$, all others). Symbols represent means \pm SE; *significant difference from static ($P < 0.05$).

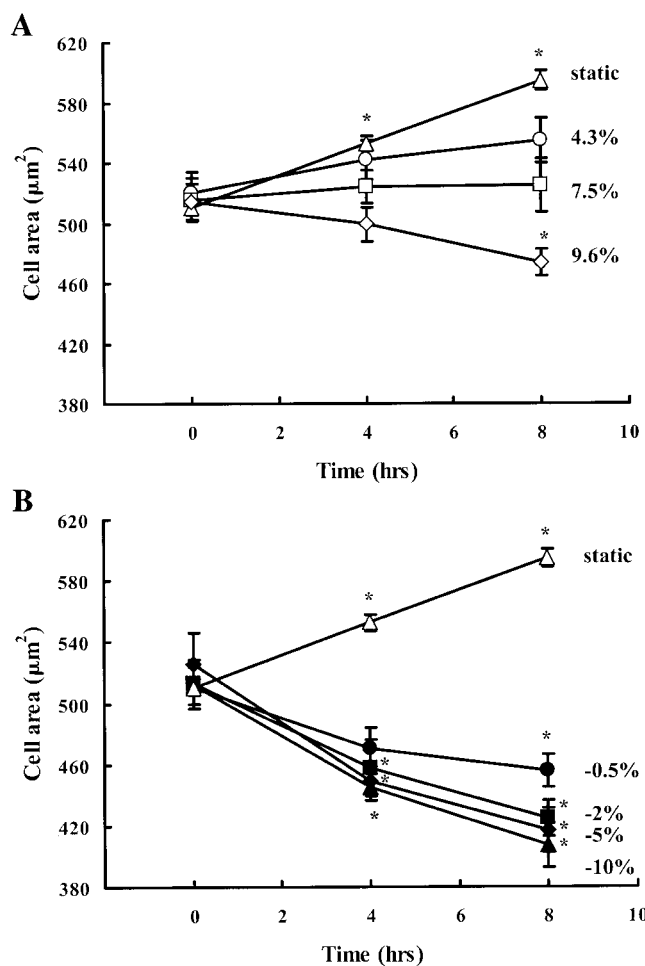


Fig. 12. Cyclic elongation (A) and cyclic compression (B) inhibit cell spreading at the wound edge of 16HBE140⁻ cells. Cells at the wound edge were traced by use of Metamorph image analysis software, and cell area was calculated. Symbols represent means \pm SE; *significant difference from initial value ($P < 0.05$, $n = 420$ for static; $n = 60$ for all others). A: static (Δ), and 4.3% (\circ), 7.5% (\square), and 9.6% (\diamond) elongation. B: static (Δ), and -0.5% (\bullet), -2% (\square), -5% (\blacklozenge), and -10% (\blacktriangle) compression.

mote cell adhesion. Although many commercially available silicone elastomer materials have been previously used for cell culture, we found little cell adhesion to our untreated custom-manufactured membranes. Surface modification with an oxygen plasma followed by attachment of functionalized amino groups significantly improved cell adhesion and growth on the substrate. Although a simple amine was used in this work, the surface modification is amenable to further manipulation such as preadsorption of extracellular matrix molecules (e.g., collagens, vitronectin) and covalent coupling of peptides (23), growth factors (16), and other molecules of biological interest. The combination of the detailed mechanical analysis, uniform strain distribution, and versatility of the surface chemistry provides a robust system for studying the associated effects of mechanical stretch and receptor-ligand interactions with the present device.

In the airways, maintenance of a continuous epithelium is important for resistance against infection and injury, control of lung fluid balance, and regulation of airway tone. Our laboratory (24) showed that release of PGE₂ by 1HAEo⁻ cells stretched by using the biaxial strain device was inhibited to the same extent as the release of PGE₂ by other airway epithelial cells strained using the Flexercell device. We have also begun to study the mechanisms by which epithelial wound closure occurs on a substrate undergoing cyclic elongation or compression as occurs in vivo. In the present study, we demonstrated that uniform biaxial elongation (10%) inhibits epithelial wound closure (Fig. 10) in a manner similar to what our laboratory previously observed with the Flexercell device (25). We also demonstrated that the extent of inhibition depends on the magnitude of elongation or compression (Fig. 11) and that cell spreading at the wound edge is dependent on the magnitude of strain (Fig. 12). With our new device, we were able to apply cyclic compression by culturing cells on a prestressed membrane and then allowing cyclic relaxation of the membrane. This is the first demonstration that the magnitude of cyclic strain affects the extent of cell spreading and wound closure.

In summary, we have presented the mechanical design of a novel biaxial strain device and custom-manufactured membrane that can be used to apply homogeneous, isotropic strain to cultured cells. We characterized the mechanical properties and the surface chemistry of the membrane, used finite element analysis to predict the appropriate geometry for uniform strain, and measured the strain field experimentally. Finally, we applied cyclic biaxial strain to cultured airway epithelial cells and measured responses similar to those we obtained using the Flexercell device, and we extended our studies by evaluating the relationship between strain magnitude and inhibition of wound closure.

We gratefully acknowledge the technical assistance of Tia Jensen.

This work was supported by the National Science Foundation (BES-9996421, to C. M. Waters), National Heart, Lung, and Blood Institute Grant HL-64981 (to C. M. Waters), and National Center for Research Resources Grant RR-01296 (to D. G. Castner).

REFERENCES

1. **Andersen KL and Norton LA.** A device for the application of known simulated orthodontic forces to human cells in vitro. *J Biomech* 24: 649–654, 1991.
2. **Baskin L, Howard PS, and Macarak E.** Effect of mechanical forces on extracellular matrix synthesis by bovine urethral fibroblasts in vitro. *J Urol* 150: 637–641, 1993.
3. **Brown TD.** Techniques for mechanical stimulation of cells in vitro: a review. *J Biomech* 33: 3–14, 2000.
4. **Brunette DM.** Mechanical stretching increases the number of epithelial cells synthesizing DNA in culture. *J Cell Sci* 69: 35–45, 1984.
5. **Carano A and Siciliani G.** Effects of continuous and intermittent forces on human fibroblasts in vitro. *Eur J Orthod* 18: 19–26, 1996.
6. **Cheng GC, Briggs WH, Gerson DS, Libby P, Grodzinsky AJ, Gray ML, and Lee RT.** Mechanical strain tightly controls fibroblast growth factor-2 release from cultured human vascular smooth muscle cells. *Circ Res* 80: 28–36, 1997.
7. **Dartsch PC and Hammerle H.** Orientation response of arterial smooth muscle cells to mechanical stimulation. *Eur J Cell Biol* 41: 339–346, 1986.
8. **Davies PF.** Flow-mediated endothelial mechanotransduction. *Physiol Rev* 75: 519–560, 1995.
9. **Ferguson GS, Chaudhry MK, Biebuyck HA, and Whitesides GM.** Monolayers on disordered substrates: self-assembly of alkyltrichlorosilanes on surface-modified polyethylene and poly(dimethylsiloxane). *Macromolecules* 26: 5870–5875, 1993.
10. **Gilbert JA, Weinhold PS, Banes AJ, Link GW, and Jones GL.** Strain profiles for circular cell culture plates containing flexible surfaces employed to mechanically deform cells in vitro. *J Biomech* 27: 1169–1177, 1994.
11. **Gorfien SF, Howard PS, Myers JC, and Macarak EJ.** Cyclic biaxial strain of pulmonary artery endothelial cells causes an increase in cell layer-associated fibronectin. *Am J Respir Cell Mol Biol* 3: 421–429, 1990.
12. **Gorfien SF, Winston FK, Thibault LE, and Macarak EJ.** Effects of biaxial deformation on pulmonary artery endothelial cells. *J Cell Physiol* 139: 492–500, 1989.
13. **Grainger DW and Healy KE.** Surface analysis of polymers and metals. In: *Handbook of Biomaterials Evaluation* (2nd ed.), edited by von Recum AF. Washington, DC: Taylor and Francis, 1998.
14. **Gruenert DC, Finkbeiner WE, and Widdicombe JH.** Culture and transformation of human airway epithelial cells. *Am J Physiol Lung Cell Mol Physiol* 268: L347–L360, 1995.
15. **Hung CT and Williams JL.** A method for inducing equi-biaxial and uniform strains in elastomeric membranes used as cell substrates. *J Biomech* 27: 227–232, 1994.
16. **Kuhl PR and Griffith-Cima LG.** Tethered epidermal growth factor as a paradigm for growth factor-induced stimulation from the solid phase. *Nat Med* 2: 1022–1027, 1996.
17. **Lee AA, Delhaas T, Waldman LK, MacKenna DA, Villarreal FJ, and McCulloch AD.** An equibiaxial strain system for cultured cells. *Am J Physiol Cell Physiol* 271: C1400–C1408, 1996.
18. **Liu M, Skinner SJ, Xu J, Han RN, Tanswell AK, and Post M.** Stimulation of fetal rat lung cell proliferation in vitro by mechanical stretch. *Am J Physiol Lung Cell Mol Physiol* 263: L376–L383, 1992.
19. **Liu M, Xu J, Souza P, Tanswell B, Tanswell AK, and Post M.** The effect of mechanical strain on fetal rat lung cell proliferation: comparison of two- and three-dimensional culture systems. *In Vitro Cell Dev Biol Anim* 31: 858–866, 1995.
20. **Moore JE Jr, Burki E, Suci A, Zhao S, Burnier M, Brunner HR, and Meister JJ.** A device for subjecting vascular endothelial cells to both fluid shear stress and circumferential cyclic stretch. *Ann Biomed Eng* 22: 416–422, 1994.
21. **Norton LA, Andersen KL, Arenholt-Bindslev D, Andersen L, and Melsen B.** A methodical study of shape changes in human oral cells perturbed by a simulated orthodontic strain in vitro. *Arch Oral Biol* 40: 863–872, 1995.

22. **Ratner BD and McElroy BJ.** Electron spectroscopy for chemical analysis: applications in the biomedical sciences. In: *Spectroscopy in the Biomedical Sciences*, edited by Gendreau RM. Boca Raton, FL: CRC Press, 1986, p. 107–147.
23. **Rezania A, Thomas CH, Branger AB, Waters CM, and Healy KE.** The detachment strength and morphology of bone cells contacting materials modified with a peptide sequence found within bone sialoprotein. *J Biomed Mater Res* 37: 9–19, 1997.
24. **Savla U, Sporn PH, and Waters CM.** Cyclic stretch of airway epithelium inhibits prostanoid synthesis. *Am J Physiol Lung Cell Mol Physiol* 273: L1013–L1019, 1997.
25. **Savla U and Waters CM.** Mechanical strain inhibits repair of airway epithelium in vitro. *Am J Physiol Lung Cell Mol Physiol* 274: L883–L892, 1998.
26. **Schaffer JL, Rizen M, L'Italien GJ, Benbrahim A, Megerman J, Gerstenfeld LC, and Gray ML.** Device for the application of a dynamic biaxially uniform and isotropic strain to a flexible cell culture membrane. *J Orthop Res* 12: 709–719, 1994.
27. **Sotoudeh M, Jalali S, Usami S, Shyy JY, and Chien S.** A strain device imposing dynamic and uniform equi-biaxial strain to cultured cells. *Ann Biomed Eng* 26: 181–189, 1998.
28. **Sumpio BE, Banes AJ, Levin LG, and Johnson G Jr.** Mechanical stress stimulates aortic endothelial cells to proliferate. *J Vasc Surg* 6: 252–256, 1987.
29. **Sumpio BE, Banes AJ, Link WG, and Johnson G Jr.** Enhanced collagen production by smooth muscle cells during repetitive mechanical stretching. *Arch Surg* 123: 1233–1236, 1988.
30. **Terracio L, Miller B, and Borg TK.** Effects of cyclic mechanical stimulation of the cellular components of the heart: in vitro. *In Vitro Cell Dev Biol* 24: 53–58, 1988.
31. **Tschumperlin DJ and Margulies SS.** Equibiaxial deformation-induced injury of alveolar epithelial cells in vitro. *Am J Physiol Lung Cell Mol Physiol* 275: L1173–L1183, 1998.
32. **Vandenburgh HH.** A computerized mechanical cell stimulator for tissue culture: effects on skeletal muscle organogenesis. *In Vitro Cell Dev Biol* 24: 609–619, 1988.
33. **Vandenburgh HH and Karlisch P.** Longitudinal growth of skeletal myotubes in vitro in a new horizontal mechanical cell stimulator. *In Vitro Cell Dev Biol* 25: 607–616, 1989.
34. **Waters CM, Chang JY, Glucksberg MR, DePaola N, and Grotberg JB.** Mechanical forces alter growth factor release by pleural mesothelial cells. *Am J Physiol Lung Cell Mol Physiol* 272: L552–L557, 1997.
35. **Waters CM and Savla U.** Keratinocyte growth factor accelerates wound closure in airway epithelium during cyclic mechanical strain. *J Cell Physiol* 181: 424–432, 1999.
36. **Winston FK, Macarak EJ, Gorfien SF, and Thibault LE.** A system to reproduce and quantify the biomechanical environment of the cell. *J Appl Physiol* 67: 397–405, 1989.

